Development of flexible ZnO thin film surface acoustic wave strain sensors on ultrathin glass substrates

Jinkai Chen[1], Hongwei Guo[1], Xingli He[1], Wenbo Wang[1], Weipeng Xuan[1], Hao Jin[1*], Shurong Dong[1], Xiaozhi Wang[1],Yang Xu[1], Shisheng Lin[1], Sean Garner[2], and Jikui Luo[3,1*]

1.Coll. of Info. Sci. & Electron. Eng., Zhejiang University, 38 Zheda Road, Hangzhou 310027, China.

2. Corning Incorporated, One River Front Plaza, Corning, NY 14831, USA

3. *Inst. of Renew. Energy & Environ. Technol., Bolton University, Deane Road, Bolton BL3 5AB, UK*

Abstract: Flexible surface acoustic wave strain sensors made on ZnO/ultrathin glass (100 μm) substrates have been developed. The sensitivity of the SAW strain sensors under different strain angles and annealing temperatures, as well as the mechanical stability are investigated. It showed that the thickness of ZnO has a strong effect on the sensitivity of the strain sensors, and thicker ZnO makes sensors with better performance. Thermal annealing at a temperature up to 200 °C also improves the sensitivity of the strain sensor significantly. Temperature coefficient of frequency maintains unchanged under different strains, showing good thermal stability. Cyclic bending test with the strain varied between zero and 2000 με exhibits good mechanical stability and reliability of the SAW strain sensors. All the results demonstrate a great potential of the flexible SAW strain sensors for flexible electronic applications.

Keywords: surface acoustic wave, strain sensors, flexible glass, annealing effect

1. Introduction

Emerging flexible electronics technologies are very attractive for many applications such as healthcare, internet of things, wearable devices *etc*. Recently, many innovative flexible electronic devices have been developed such as flexible batteries[1], flexible organic flash memory[2], electronic skin[3], flexible sensor array[4], flexible surface acoustic wave and film bulk acoustic resonators[5] *etc*. The flexibility of devices is largely determined by the properties of

the substrate material. Depending on application, many kinds of flexible substrates have been explored. Among them, polymers such as polyethylene terephthalate (PET), polyimide (PI) and polymethyl methacrylate (PMMA) *etc* are the most popular ones and have been intensively investigated for flexible electronics applications[5-7]. Polymers can endure extremely large strains, but suffer from the shortages of low transparency, poor thermal stability, poor mechanical strength and reliability *etc*. Glass substrates have excellent transparency and mechanical strength, but the low flexibility of normal rigid glass substrates limits their applications in flexible electronics. The recently developed ultrathin flexible Corning® Willow Glass has the combined merits of good flexibility, high transparency, excellent corrosion and wear resistance, mechanical reliability and thermal stability, thus has raised great interests for the fabrication of flexible electronic devices[8-13].

Surface acoustic wave (SAW) devices are widely used in modern electronics and sensing. Sensors based on SAW devices attract increasing interests in research and for commercial applications. SAW sensors can be used in various areas to monitor environmental changes such as temperature, pressure[14], humidity[6,15], strain[8,16], ultraviolet light[17] *etc*. Also, traces of chemicals and biological samples can also be detected with assistance of different kinds of functional layers on the surface of SAW devices[18,19]. Recently, we have developed flexible SAW devices on PI[6,20], PET[7] and Willow Glass[8], and demonstrated high performance humidity, UV-light and strain sensors. All the flexible SAW sensors showed comparable performance to the devices on solid substrates, demonstrated their great potential for flexible applications.

Here we report further investigation on the effects of zinc oxide (ZnO) piezoelectric layer thickness, annealing temperature and strain alignment angle on the properties of the flexible glass-based SAW strain sensors. It shows that the strain sensor has the best sensitivity when the strain angle is ~45° with the SAW propagation direction. The sensors with a thicker ZnO layer, being annealed at 200 °C have better performance.

2. Modeling of SAW strain sensor

For SAW-based strain sensors, frequency shift is normally utilized to assess the strain applied. The strain-induced frequency shift has two components: (1) the deformation of interdigitated transducers (IDTs) which leads to change of the wavelength; and (2) the change of acoustic velocity of the materials involved due to the applied stress. These two effects can

be considered independently, and the overall sensitivity of the strain sensors can be calculated by combining these two effects together.

2.1 IDT deformation induced wavelength change

Figure 1(a) shows the schematic of our SAW strain sensors. The angle between the SAW propagation direction and applied strain direction is defined as θ as indicated in Figure 1(a). Although a stress applied perpendicular to the SAW propagation will induce a deformation of the device along the SAW propagation direction as well, as determined by the Poisson constant, it is minor, therefore for simplicity, only the component of the strain along the SAW propagation direction is considered to influence the wavelength of the device. The sensitivity (S_w) induced by wavelength change can be defined as follows,

$$S_w = \mu\frac{f_a - f_b}{\varepsilon} = \mu\frac{\frac{v}{\lambda_a} - \frac{v}{\lambda_b}}{\varepsilon} = \mu\frac{\frac{v}{\lambda_b(1+\varepsilon\cos\theta)} - \frac{v}{\lambda_b}}{\varepsilon} = -\mu\frac{v\cos\theta}{\lambda_b(1+\varepsilon\cos\theta)}, \quad 0 \le \theta \le \frac{\pi}{2} \tag{1}$$

where f_a, f_b is the resonant frequency after and before applying strain, λ_a, λ_b the SAW wavelength after and before applying strain, ε, v the applied strain and acoustic velocity, respectively. μ is a constant with a value of 10^{-6}.

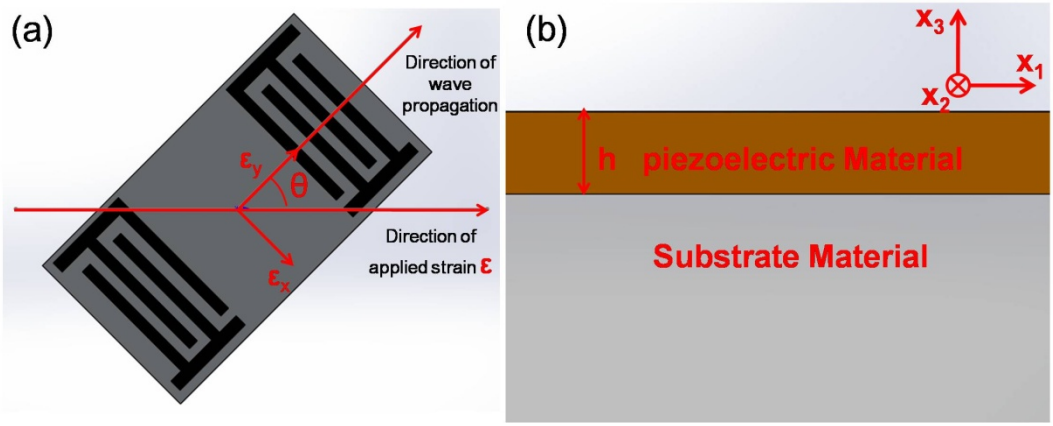

FIG. 1. (a) Schematic of a SAW device and the applied strain with an alignment angle θ with the SAW propagation direction. (b) Cross section of the layered SAW structure and coordination. h is the thickness of the piezoelectric material.

2.2 Strain-induced velocity change

The velocity change under applied stress could be calculated by a modified form of equations of motion which consider the perturbation of applied strain[21]. In a stressed piezoelectric medium, the equations are,

$$\sigma_{ik}u_{j,ki} + c_{ijkl}u_{k,li} + e_{kij}\varphi_{,ki} = \rho\ddot{u}_j, \quad (j = 1,2,3) \tag{2}$$

and

$$e_{ikl}u_{k,li} - \epsilon_{ik}\varphi_{,ki} = 0 \tag{3}$$

Where σ_{ik} is the initial stress, ρ the mass density, u the mechanical displacement, and φ the electric potential, c_{ijkl} the elastic stiffness tensor, e_{ijk} the piezoelectric tensor and ϵ_{ij} the dielectric tensor. The subscripts i, j, k, l take the value of 1, 2 and 3, referred to the coordinate system as shown in Figure 1(b). The substrate material is approximated for a half space as its thickness (~100 μm) is much larger than the thickness (h) of the piezoelectric layer (< 3.5 μm). x_1 represents the direction of SAW propagation.

A solution for the SAW displacement vector is a linear combination of fundamental solutions of the form[22],

$$u_k = e^{j\omega t}\beta_k exp\left[-j\frac{\omega}{v}\sum_{m=1}^{3}\gamma_m x_m\right], \qquad (k = 1, 2, 3, 4) \tag{4}$$

$\gamma_1 \stackrel{\text{def}}{=} 1$, $\gamma_2 \stackrel{\text{def}}{=} 0$, $and\ \gamma_3$ is a complex normalized transverse wave number, and v is the velocity of the SAW. Here u_4 represents φ for convenience.

Substituting eq.(4) into eq.(2) and eq.(3), a linear homogeneous equation can be obtained. There are only σ_{11}, σ_{13}, σ_{33} left after substitution, because γ_2 equals to zero. The determinant of these four equations with the four variables β_1, β_2, β_3, and β_4, must be zero for nontrivial solution. Then we will obtain an eight-order polynomial equation in γ_3. There are totally 8 different roots of $\gamma_3^{(q)}$, q = 1 to 8, and for each $\gamma_3^{(q)}$, four relevant $\beta_k^{(q)}$ could be found. In the layered material, all eight $\gamma_3^{(q)}$ are useful. But in the substrate at most four values of $\gamma_3^{(q)}$ which have a positive imaginary part, are meaningful because of the attenuation of the acoustic wave in the substrate. Then the complete solution is given by,

$$u_{k(L)} = \sum_{q=1}^{Q(L)} B_{(L)}^{(q)}\beta_{k(L)}^{(q)} exp\left[\left(-j\frac{\omega}{v}\right)\sum_{m=1}^{3}\gamma_{m(L)}^{(q)}x_m\right], \ Q(L) \leq 8 \tag{5}$$

for the piezoelectric layer, and

$$u_{k(S)} = \sum_{q=1}^{Q(S)} B_{(S)}^{(q)}\beta_{k(S)}^{(q)} exp\left[\left(-j\frac{\omega}{v}\right)\sum_{m=1}^{3}\gamma_{m(S)}^{(q)}x_m\right], \quad Q(S) \leq 4 \tag{6}$$

for the substrate.

The boundary conditions are as follow[23],

(1) Continuity of particle displacement and electric potential at the interface between the thin

piezoelectric layer and the substrate.

(2) Continuity of normal stress and electric displacement components at the interface between the thin piezoelectric layer and the substrate.

(3) Zero traction force at the free surface of the piezoelectric layer

(4) The continuity of u_4 and D_3 at $x_{3(L)} = 0$ and u_4 vanishes at $x_{3(L)} = h$.

The boundary conditions form a set of 12 homogeneous equations for four variables $B_{(S)}^{(q)}$ and eight variables $B_{(L)}^{(q)}$. The determinant of these equation sets should be zero for nontrival solutions. Then a transcendental equation for the determination of v is obtained. An iterative process was used in computing to find the v.

The applied strain not only modifies the equation of motion, but also perturbs the material constants. There are three main independent perturbed material constants influencing the acoustic velocity under stress[24], which are the initial stress (σ_{ij}), material elastic constants (c_{ijkl}), and material density (ρ). The original parameters were substituted with these changed ones to calculate the velocity change under different strains and applied angles.

The sensitivity (S_v) induced by velocity change can be calculated using the fractional change in velocity ($\frac{v_a - v_b}{v_b \varepsilon}$) calculated above,

$$S_v(Hz/\mu\varepsilon) = \mu \frac{f_a - f_b}{\varepsilon} = \mu \frac{\frac{v_a}{\lambda} - \frac{v_b}{\lambda}}{\varepsilon} = \mu \frac{v_a - v_b}{\lambda \varepsilon} \quad (7)$$

3. Experimental

A 100 μm thick ultrathin Willow Glass substrate was used for the fabrication of SAW strain sensors. The ZnO piezoelectric thin films were deposited on the glass substrates using a direct-current (DC) reactive magnetron sputtering with a Zn target (purity of 99.99%). The optimized sputtering conditions for the pressure, power, substrate temperature, bias voltage and gas flow ratio of Ar/O_2 were 1.0 Pa, 180 W, 90 °C, -75 V and 100/50 sccm, respectively. The IDTs were formed using the conventional ultraviolet light photolithograph and lift-off process. An aluminum (Al) thin film (~100 nm) was then deposited by sputtering on the patterned surface of ZnO, and the samples were immersed into acetone to dissolve the photoresist and form the IDTs. The sputtering pressure, power and flow rate of Ar for Al deposition were 0.5 Pa, 200 W, 100 sccm, respectively. To investigate the annealing effect on

the performance of the sensors, the ZnO substrates were annealed by rapid thermal annealing (RTP-CT100M) in N_2 at atmospheric pressure for 10 min for each temperature. Figure 2(a) shows the fabricated devices on a glass wafer, showing its good flexibility and transparency.

The measurement setup for strain sensing experiments was explained in our previous work[8]. The bare SAW device (3 mm × 4mm) was glued (3M RITE-LOK PR40) on a flexible steel bar. Then the electrodes of the devices were bonded to a flexible PCB board, which was also glued on the steel bar, using the conductive adhesive (MCN-DJ002) and electrically connected to Sub Miniature version A (SMA) connectors. For measuring the strain, a standard full-bridge strain gauge (BF1000-3h, 5mm × 5mm) was glued paralleled to the PCB board. A computer was used to capture the strain gauge data through electrical connects. A robotic arm (HSV-500) was used to bend the steel bar with the strain gauge and SAW device, and the device was electrically connected to a vector network analyzer (E5071C) to measure the transmission properties of the SAW sensors. A LabVIEW based program was developed to implement automated measurements of frequency shift of the device. Figure 2(b) shows the setup for the temperature stability tests. The steel bar with the SAW device and strain gauge were placed in the temperature-humidity controlled chamber and the electrical connections were the same as mentioned above to measure its sensitivity under different temperatures and strains.

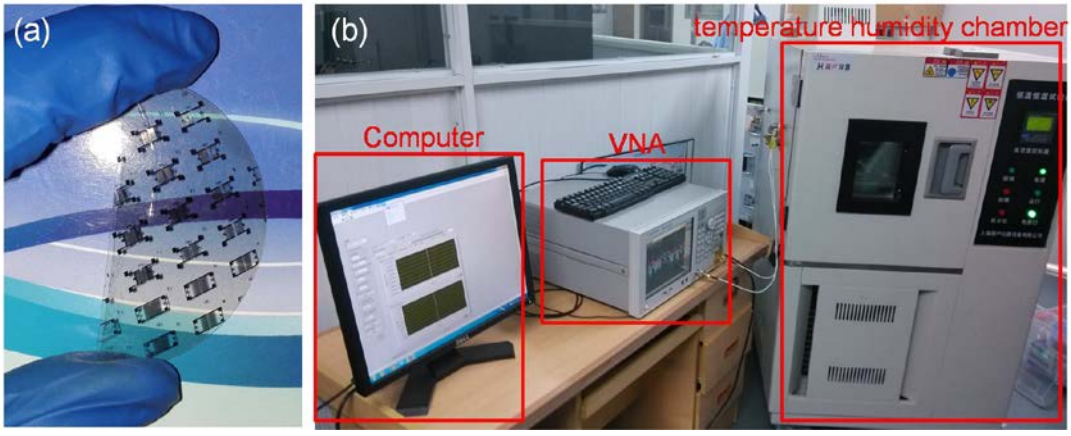

FIG. 2. (a) Fabricated SAW devices on an ultrathin Willow Glass substrate, showing good flexibility and transparency. (b) The setup for temperature stability measurement. Strain sensors were placed inside the temperature-humidity controlled chamber.

4. Results and discussion

4.1 Angle, thickness, annealing-temperature dependence of sensitivity

The sensitivity of a SAW strain sensor changes when the angle of the applied strain with the SAW propagation varies, and this has been demonstrated by Donohoe *et al* for the SAW strain sensors on AT-X quartz[16]. As shown in Figure 1(a), any strain ε applied to the SAW can be divided into two parts, ε_x (perpendicular to the direction of SAW propagation) and ε_y (parallel to the direction of SAW propagation). It is the ε_x and ε_y strains that change the material constants (σ_{ij}, E, c_{ijkl}, ρ, λ), and affect the sensitivity of the SAW strain sensors. Figure 3(a) is the sensitivity of the SAW strain sensor (wavelength λ = 16 μm, the thickness of ZnO is 2μm) as a function of strain angle. The measured sensitivity is 76.6 Hz/με, 99.3 Hz/με, 100.0 Hz/με, 21.1 Hz/με and -28.5 Hz/με for 0°, 30°, 45°, 80° and 90° strain angle, respectively. The total sensitivity and each contribution from the two components are also illustrated in Figure 3(a) for clarity. The simulated sensitivity induced by velocity change is positive, with the largest sensitivity occurring at the angle of approximately 30°. The sensitivity induced by the wavelength change is negative, but it decreases monotonically with the increase in strain angle. At 90°, there is no wavelength change induced sensitivity variation as the bending perpendicular to the wave propagation direction does not change the pitch size of the IDTs. The simulated total sensitivity of the strain sensors can be calculated by adding these two separated sensitivities together. When these two effects are combined, the largest over-all simulated sensitivity occurs at the angle of 45°. The simulation and experimental results have a similar tendency with the change of strain angle. The sensitivities increase with the increase in angle and then decrease when the angle is larger than 45°. The agreement between the simulation and measurement is good for angles smaller than 60°, and the deviation becomes larger at large strain angles. This is due partially to the error in measuring the strain angle and partially to the deviation of the material constants of practical materials from those of ideal material constants of ZnO and glass substrate. The material constants of the monocrystalline ZnO were used in the modeling for the polycrystalline ZnO films deposited by the sputtering.

Figure 3(b) shows the sensitivity of SAW strain sensors (wavelength λ = 20 μm) with different ZnO thin film thicknesses. The sensitivity is 84.5 Hz/με, 105 Hz/με and 136.6 Hz/με when the thickness of ZnO thin film is 2 μm, 2.7 μm and 3.3 μm, respectively. The improvement for the latter two is 24.3% and 61.7%, respectively. The sensitivity of SAW strain sensor increases significantly with the increase in thickness of the ZnO thin film, which can be attributed to the better crystallization of thicker ZnO film[25]. No thicker ZnO film was deposited on ultra-thin glass because of the internal stress of the ZnO films, which would fail

the devices. If low stress ZnO films can be obtained, then thicker films can be used to fabricate SAW strain sensors with better sensitivity.

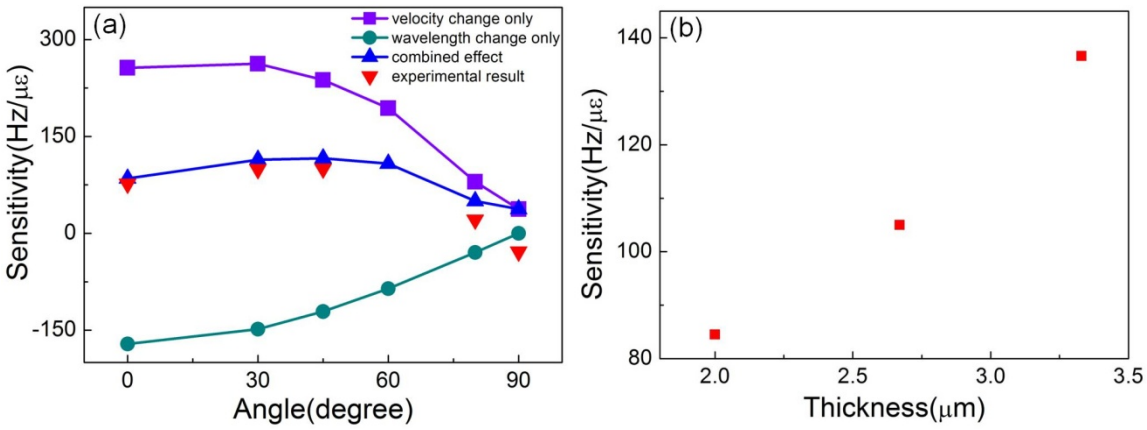

FIG. 3. (a) The simulated and experimental sensitivities of SAW strain sensors with different strain angles. (b) The sensitivity of SAW strain sensor as a function of ZnO layer thicknesses.

Figure 4 shows the annealing effect on the sensitivity of SAW strain sensor (λ = 20 μm, the ZnO thickness is 2 μm). The sensitivity of the as-made sensor is 87.8 Hz/με, and increases to 121.7 Hz/με, and 138.9 Hz/με after 150 °C and 200 °C annealing, respectively. The improvement is 38.6 % and 58.2 % respectively. The large improvement of the sensitivity is attributed to the better crystallization of ZnO after annealing, as discussed in our previous work[8]. The results demonstrate that the ultrathin glass substrate has the advantages for some flexible applications owing to the good thermal stability. The relationship between the resonant frequency shift and strain shows a good linearity which is one of very important factors for sensing applications.

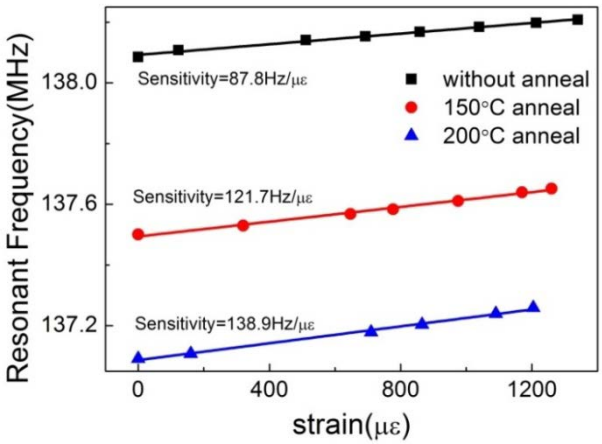

FIG. 4. Resonant frequency shift as a function of strain. The slopes represent the strain sensitivity which increases with the annealing temperature.

4.2 Reliability of the SAW strain sensor

Environmental temperature affects the performance of sensors, therefore it is necessary to investigate the temperature influence to the SAW strain sensors. The temperature coefficient of frequency (TCF) is defined as $\frac{1}{f_0}\frac{\Delta f}{\Delta T}$, where f_0, Δf and ΔT is the original resonant frequency, frequency shift and change of temperature, respectively. The TCF of the SAW strain sensor (λ = 12 μm, the thickness of ZnO is 2 μm) under different strains was measured under various temperatures. The TCF was measured with a constant relative humidity (RH) of ~50%RH. As shown in Figure 5, the TCF is -15.72 ppm/K, -16.04 ppm/K and -15.41 ppm/K with the strain of 0 με, 1400 με and 3000 με, respectively. The TCF shows a stable value with small deviation under various strains, indicating little influence by temperature which is an excellent property for practical applications. Besides, the TCF of ultrathin glass based devices is much smaller than that of the ones on PI substrates (~400 ppm/K) as reported in our previous work[6]. The relatively low TCF is even better than many SAW sensors on solid substrates[26], indicating that our devices can be used in environment with varying temperature, thus it can play a better role for sensor applications.

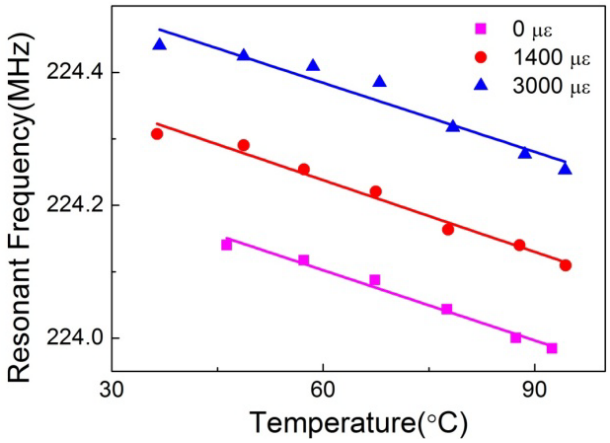

FIG. 5. Frequency shift as a function of measurement temperature under different applied strains. All show good linearity with the gradients remained almost unchanged.

A cyclic bending test was carried out to assess the mechanical reliability of the SAW strain sensor (λ = 20 μm, the thickness of ZnO is 2.7 μm, sensitivity ~110.8 Hz/με). Figure 6(a) shows the cyclic bending test results up to 938 times (6568 s) with the strain varied cyclically from 0 to 2000 με. Figure 6(b) and (c) show the details of the frequency variation at the beginning (0-300 s) and end (6268-6568 s) of the cyclic bending test, respectively. The average resonant frequency shift increases from 221.6 kHz to 227.7 kHz from the beginning to the end of the cyclic bending test. The baseline frequency of the overall bending test drifts

downward slightly (~20 kHz), which is equivalent to a strain of ~180 με over 938 times bending. Close inspection showed this is due to the slight position shift of the robotic arm and the loss of wire bonding, not the device deterioration. Nevertheless, the results show the SAW strain sensor has excellent stability and repeatability after being bent at large strain for over hundreds of times, demonstrated its great potential for applications.

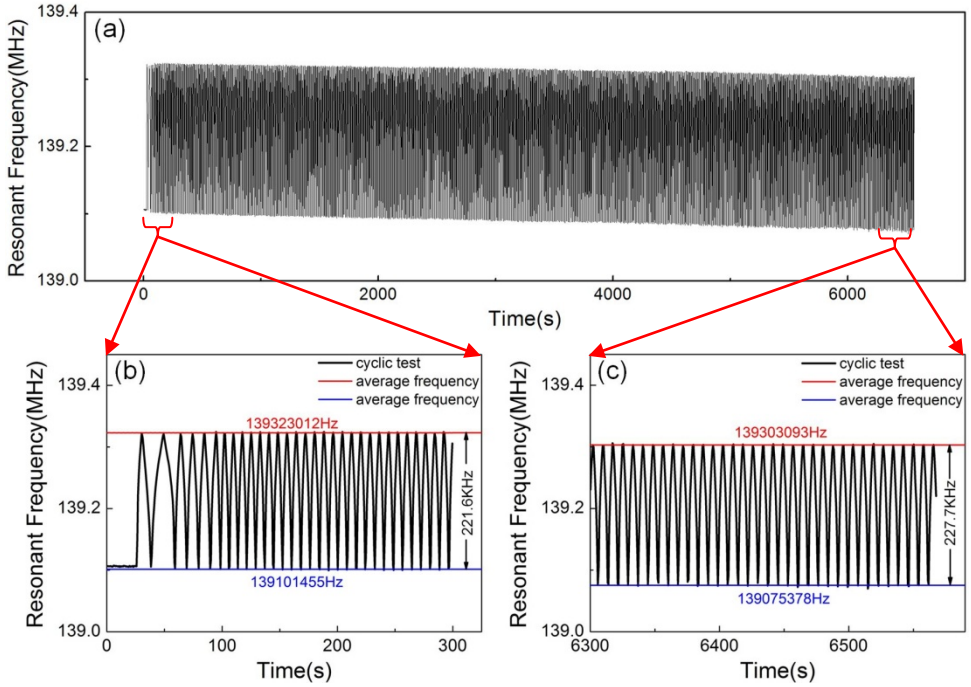

FIG. 6. (a) Frequency under cyclic bending test for 938 cycles (6568 s). The baseline frequency drifts downwards slightly with the time. (b) The beginning of the cyclic bending test (0–300 s), and (c) the end of the cyclic bending test (6268–6568 s), showing good stability for each period.

Detection limit is also one of the key issues for sensor applications. For SAW strain sensors, the upper detection limit depends on the mechanical strength of the ZnO and glass substrate which is about 3000 με (~ 5 times larger than others), reported in our previous publication[8]. We believe that the resonant frequency jittering of a SAW device is the main factor which determines the low limit of the SAW strain sensors. We have measured the resonant frequency jittering of the SAW strain sensor of 16 μm wavelength and 99.3 Hz/με sensitivity for a period of 30 min. The largest resonant frequency jittering range is 2.24 kHz, which corresponds to 22.6 με by dividing the obtained sensitivity. The applied strain must be larger than that for a clear detection, implying the low detection limit of this type of SAW strain sensor is ~22.6 με. If a proper data smoothing method is utilized, the low detection limit could be further improved, and it is under investigation.

5. Conclusions

Surface acoustic wave strain sensors based on ZnO/ultra-thin glass have been developed. The sensitivity of the SAW strain sensor under different strain angles was investigated and shows good agreement with the modeling results. The thickness of ZnO piezoelectric film has a strong effect on the sensitivity of the SAW strain sensors, and thicker ZnO makes sensors with better performance and sensitivity. Thermal annealing at modest temperature could also improve the sensitivity of the SAW strain sensor. The optimized conditions for the best sensitivity of the strain sensors are 3.3 μm ZnO thickness, 200 °C annealing and ~45° of strain angle. Temperature coefficient of frequency of the sensor remains constant under different strains, showing excellent thermal stability. Cyclic bending test at a strain from zero to 2000 με shows very excellent mechanical stability and reliability of the SAW strain sensors. All the results show brilliant sensor performance, owing to the good property of the ultrathin flexible glass substrate, hence demonstrated the great potential of the ultrathin glass-based SAW strain sensors for flexible electronic applications.

Acknowledgements

This work was supported by NSFC (No.61274037 and 61204124), Research Fund for the Doctoral Program of Higher Education of China (No. 20120101110031). The authors also would like to acknowledge the support by the Innovation Platform of Micro/Nanodevices and Integration System, Zhejiang University.

References

1 Z. Q. Wang, Z. Q. Wu, N. Bramnik, and S. Mitra, Adv. Mater. **26,** 970 (2014).

2 T. Sekitani, T. Yokota, U. Zschieschang, H. Klauk, S. Bauer, K. Takeuchi, M. Takamiya, T. Sakurai, and T. Someya, Science **326,** 1516 (2009).

3 D. H. Kim, N. S. Lu, R. Ma, Y. S. Kim, R. H. Kim, S. D. Wang, J. Wu, S. M. Won, H. Tao, A. Islam, K. J. Yu, T. I. Kim, R. Chowdhury, M. Ying, L. Z. Xu, M. Li, H. J. Chung, H. Keum, M. McCormick, P. Liu, Y. W. Zhang, F. G. Omenetto, Y. G. Huang, T. Coleman, and J. A. Rogers, Science **333,** 838 (2011).

4 N. T. Tien, S. Jeon, D. I. Kim, T. Q. Trung, M. Jang, B. U. Hwang, K. E. Byun, J. Bae, E. Lee, J. B. H. Tok, Z. N. Bao, N. E. Lee, and J. J. Park, Adv. Mater. **26,** 796 (2014).

5 G. H. Chen, X. R. Zhao, X. Z. Wang, H. Jin, S. J. Li, S. R. Dong, A. J. Flewitt, W. I. Milne, and J. K. Luo, Sci. Rep. **5** (2015).

6 X. L. He, D. J. Li, J. Zhou, W. B. Wang, W. P. Xuan, S. R. Dong, H. Jin, and J. K. Luo, J. Mater. Chem. C **1,** 6210 (2013).

7 X. L. He, H. W. Guo, J. K. Chen, W. B. Wang, W. P. Xuan, Y. Xu, and J. K. Luo, Appl. Phys.

Lett. **104** (2014).
8 J. K. Chen, X. L. He, W. B. Wang, W. P. Xuan, J. Zhou, X. Z. Wang, S. R. Dong, S. Garner, P. Cimo, and J. K. Luo, J. Mater. Chem. C **2,** 9109 (2014).
9 S. M. Garner, M. Q. He, P. Y. Lo, C. F. Sung, C. W. Liu, Y. M. Hsieh, R. Hsu, J. M. Ding, J. P. Hu, Y. J. Chan, J. J. ChiehLin, X. H. Li, M. Sorensen, J. F. Li, P. Cimo, and C. K. TingKuo, J. Disp. Technol. **8,** 590 (2012).
10 S. Hoehla, S. Garner, M. Hohmann, O. Kuhls, X. H. Li, A. Schindler, and N. Fruehauf, J. Disp. Technol. **8,** 309 (2012).
11 W. L. Rance, J. M. Burst, D. M. Meysing, C. A. Wolden, M. O. Reese, T. A. Gessert, W. K. Metzger, S. Garner, P. Cimo, and T. M. Barnes, Appl. Phys. Lett. **104** (2014).
12 S. Garner, S. Glaesemann, and X. H. Li, Appl. Phys. A-Mater. **116,** 403 (2014).
13 H. P. Mahabaduge, W. L. Rance, J. M. Burst, M. O. Reese, D. M. Meysing, C. A. Wolden, J. Li, J. D. Beach, T. A. Gessert, W. K. Metzger, S. Garner, and T. M. Barnes, Appl. Phys. Lett. **106** (2015).
14 A. Talbi, F. Sarry, L. Le Brizoual, O. Elmazria, and P. Alnot, Proceedings of the 2004 IEEE International Frequency Control Symposium and Exposition, (2005), pp. 566-570.
15 W. P. Xuan, M. He, N. Meng, X. L. He, W. B. Wang, J. K. Chen, T. J. Shi, T. Hasan, Z. Xu, Y. Xu, and J. K. Luo, Sci. Rep. **4** (2014).
16 B. Donohoe, D. Geraghty, and G. E. O'Donnell, IEEE Sens. J. **11,** 1026 (2011).
17 W. B. Wang, H. Gu, X. L. He, W. P. Xuan, J. K. Chen, X. Z. Wang, and J. K. Luo, Appl. Phys. Lett. **104** (2014).
18 Y. Wang, X. S. Du, Y. Long, X. Z. Tang, Z. Chen, and Y. D. Jiang, Sensor. Actua. B-Chem. **206,** 252 (2015).
19 F. Bender, R. E. Mohler, A. J. Ricco, and F. Josse, Anal. Chem. **86,** 1794 (2014).
20 H. Jin, J. Zhou, X. L. He, W. B. Wang, H. W. Guo, S. R. Dong, D. M. Wang, Y. Xu, J. F. Geng, J. K. Luo, and W. I. Milne, Sci. Rep. **3** (2013).
21 V. V. Bolotin, *Nonconservative problems of the theory of elastic stability* (Macmillan, New York, 1963) p.43.
22 J. J. Campbell and W. R. Jones, IEEE T. Son. And Ultrason. **Su15,** 209 (1968).
23 A. L. Nalamwar and M. Epstein, IEEE T. Son. And Ultrason. **23,** 144 (1976).
24 A. L. Nalamwar and M. Epstein, J. Appl. Phys. **47,** 43 (1976).
25 X. Y. Du, Y. Q. Fu, S. C. Tan, J. K. Luo, A. J. Flewitt, S. Maeng, S. H. Kim, Y. J. Choi, D. S. Lee, N. M. Park, J. Park, and W. I. Milne, J. Phys.: Conf. Ser. **76**, 012035 (2007).
26 W. B. Wang, X. L. He, J. Zhou, H. Gu, W. P. Xuan, J. K. Chen, X. Z. Wang, and J. K. Luo, J. Electrochem. Soc. **161,** B230 (2014).